

First-Principles DFT+U Studies of the Atomic, Electronic, and Magnetic Structure of α -MnO₂ (Cryptomelane)

Eric Cockayne* and Lan Li

Ceramics Division, Material Measurement Laboratory,

National Institute of Standards and Technology, Gaithersburg, Maryland 20899 USA

**Corresponding author. Tel: (+1) 301-975-4347; Fax: (+1) 301-975-5334; electronic address: eric.cockayne@nist.gov*

Abstract

Density functional theory DFT+U calculations are used to investigate α -MnO₂, a structure containing a framework of corner and edge sharing MnO₆ octahedra with tunnels in between. Placing K⁺ ions into the tunnels stabilizes α -MnO₂ with respect to the rutile-structure β -MnO₂ phase, in agreement with experiment. The computed magnetic structure has antiferromagnetic (ferromagnetic) Mn-Mn interactions between corner-sharing (edge-sharing) octahedra. Pure α -MnO₂ is found to be a semiconductor with an indirect band gap of 1.3 eV. Water and related hydrides (OH⁻; H₃O⁺) can also be accommodated in the tunnels; the equilibrium K-O distance increases with increasing oxygen hydride charge. Including van der Waals interactions improves the agreement between the calculated monoclinic distortion and experimental value, but does not improve the volume

1. Introduction

Manganese dioxide (MnO₂)-based materials are of great interest for various applications, ranging from catalysts and batteries to energy efficient devices and carbon storage applications [1-6]. Mn is multivalent, and thus forms oxides of several different stoichiometries [7]. For MnO₂ phases, the oxidation state is Mn⁴⁺. The equilibrium phase of MnO₂ at standard temperature and pressure is β -MnO₂ [7], or pyrolusite [8], with the rutile structure, but several metastable phases are also known.

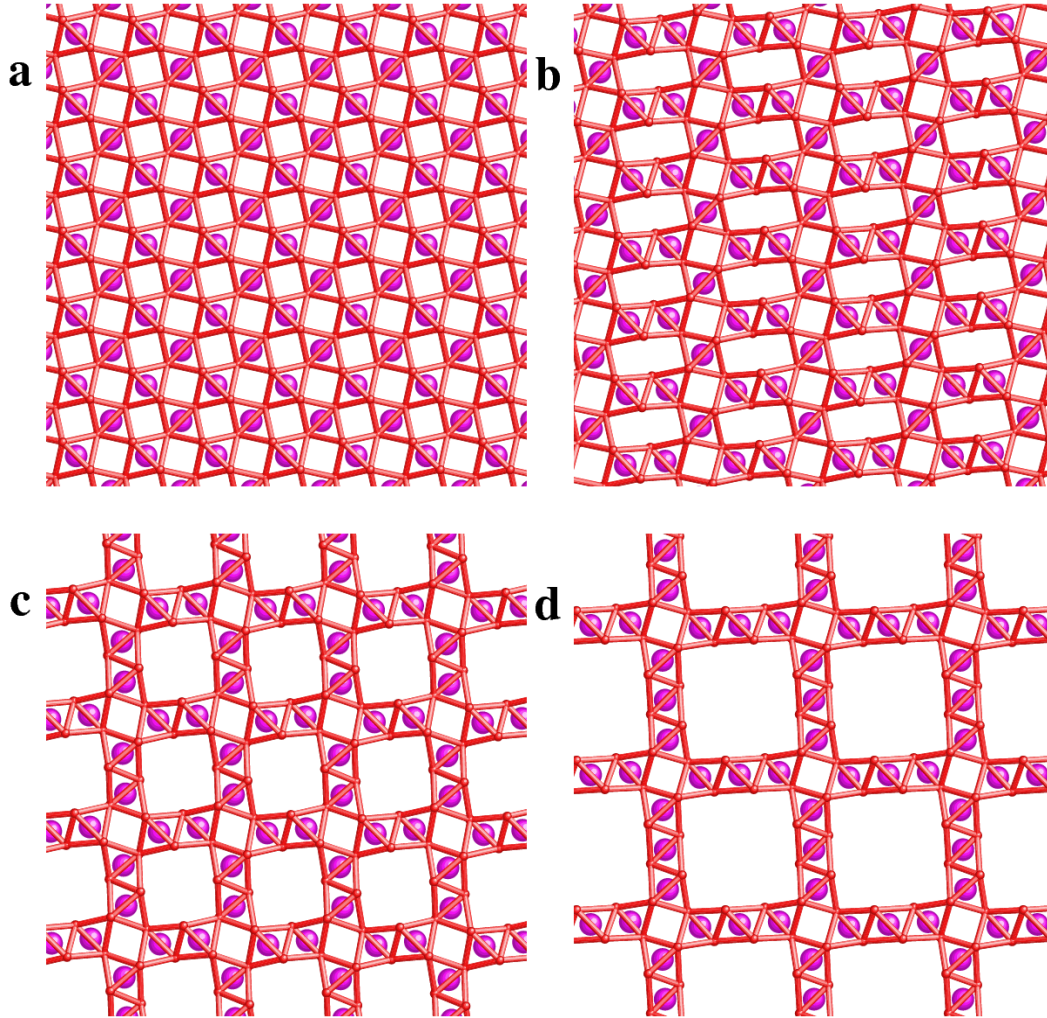


Fig. 1 Octahedral molecular sieve MnO_2 structures with alternating 1×1 and $m \times n$ tunnels. (a) $m=1, n=1$ $\beta\text{-MnO}_2$ structure. (b) $m=2, n=1$. (c) $m=2, n=2$ $\alpha\text{-MnO}_2$ structure. (d) $m=3, n=3$. Mn atoms shown in purple and oxygen octahedral frameworks in red.

In fact, MnO_2 forms the framework of an entire family of “octahedral molecular sieve” (OMS) structures (Fig. 1) [4,9]. The building blocks of these structures are columns of edge-sharing MnO_6 octahedra. These columns join either corner-to-corner or edge-to-edge. As shown in Fig. 1, MnO_2 can form an infinite number of OMS structures with alternating (1×1) tunnels and $(m \times n)$ tunnels. The $m=1, n=1$ OMS structure is $\beta\text{-MnO}_2$. The $m=2, n=2$ OMS structure is the well-known $\alpha\text{-MnO}_2$ phase [8]. Careful studies of $\alpha\text{-MnO}_2$ show that the structure generally contains additional species, such as cations ($\text{K}^+, \text{Pb}^{2+}, \text{Ba}^{2+}$, etc.), or water molecules [8-10] inside the 2×2 tunnels. The presence of these additional species offers an opportunity to design MnO_2 OMS materials with tailored properties. Depending on which species are present, $\alpha\text{-MnO}_2$ is known by various names such as hollandite or cryptomelane [8-9]. In this work, we focus on the K^+ containing, or cryptomelane variant.

To fully exploit the properties of MnO₂ OMS materials, a fundamental understanding of their atomic and electronic structure is needed. In recent years, there have been considerable experimental studies using Raman scattering spectroscopy, X-ray diffraction, and X-ray photoelectron spectroscopy [11-13]. Theoretical studies can complement these experimental observations. In particular, first-principles density functional theory (DFT) calculations can uncover the electronic origin of structure-property relationships in these advanced materials. In this work, we use DFT calculations to investigate the structure and energetics of MnO₂ OMS materials, in particular α -MnO₂.

The paper is organized as follows. In Sec. 2, we present the computational methods and discuss the treatment of Mn magnetism within DFT. In Sec. 3 and 4, we present our results and conclusions on the atomic, electronic, and magnetic structure of α -MnO₂, with and without additional species present that, for simplicity, we term “dopants” in this work.

2. Computational Methods

Structural and electronic structure calculations were performed using the Vienna *Ab initio* Simulation Package (VASP) code [14] based on self-consistent density functional theory (DFT). We used projector-augmented wave pseudopotentials [15] in conjunction with a plane wave expansion of the wavefunctions. The generalized gradient approximation (GGA) was used to approximate the exchange and correlation functional, using the recently-developed PBEsol (Perdew-Burke-Ernzerhof revised for solids [16]) parameterization.

We utilized convergence tests to select the k -point mesh size and plane-wave energy cutoff. Structural geometries and forces were well-converged for a $2\times 6\times 2$ Monkhorst-Pack grid and a 400 eV cutoff. An $8\times 24\times 8$ Monkhorst-Pack mesh was used for density of state (DOS) calculations. A Gaussian smearing of 0.05 eV was used for the Fermi surface broadening. Relaxations of atomic positions and lattice vectors were performed until residual forces were 0.01 eV/Å or less.

Because Mn⁴⁺ is a magnetic ion, it is crucial to include the effects of magnetism in electronic structure studies of manganese oxides. Previous works have shown that the exchange-correlational approach used within DFT has a large effect on the computed electronic structure and the magnetic ordering of manganese oxides [17]. These studies predated the PBEsol version of GGA. Using PBEsol for exchange and correlation, we first revisited β -MnO₂ within the GGA+U(+J) approach for magnetism. The experimentally-known magnetic structure for β -MnO₂ is straightforward: the Mn-Mn interaction for corner-sharing MnO₆ octahedra is antiferromagnetic [18] due to superexchange. This completely determines the magnetic structure, as shown in Fig. 2(a). Remarkably, using the GGA+U+J approach of Liechtenstein *et al.* [19], we were able to reproduce both the band gap = 0.27 eV [20] and the unit cell volume [10] simultaneously by using reasonable values for the effective Mn on-site Coulomb (U) and exchange (J)

values of 2.8 eV and 1.2 eV, respectively. These parameters are assumed to be transferrable to Mn^{4+} ions in other geometries such as $\alpha\text{-MnO}_2$.

Although the focus of this work is on the basic properties of cryptomelane, inclusion of van der Waals (vdW) interactions [21] will be crucial in future studies of carbon capture in this material, and are expected to quantitatively affect the results even for dopants such as K^+ and water whose charge and dipole interactions are expected to be much stronger than their vdW interactions. We therefore tested vdW DFT calculations on cryptomelane for comparison with non-vdW calculations, using the optBB86b functional [22] as encoded in VASP [22]. The magnetic parameters were reoptimized on $\beta\text{-MnO}_2$ ($U = 2.0$ eV, $J = 1.0$ eV for Mn d; $U = 2.1$ eV, $J = 0.0$ eV for O p).

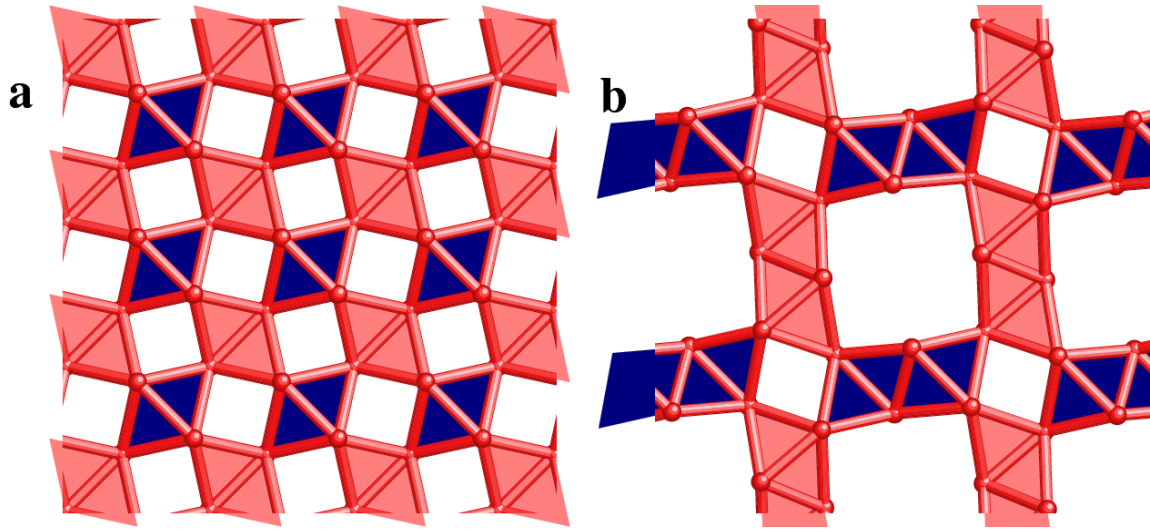


Fig. 2 (a) Experimental magnetic structure of $\beta\text{-MnO}_2$. (b) Predicted ground state magnetic structure of $\alpha\text{-MnO}_2$. Octahedra are colored according to the spin state of the central Mn, dark blue for spin "up" and light red for spin "down". All octahedra in each column have the same spin.

The density of states (DOS) and projected density of states (PDOS) show the electronic structure of $\alpha\text{-MnO}_2$ and how it is affected by dopants. In VASP, the PDOS is obtained via projecting the DOS in spheres of Wigner radii centered at nuclei. Both are spin-dependent in our calculations. The total DOS is the sum of the spin-up and spin-down DOS. All calculations were done for neutral cells. When charges are given for dopant ions, e.g. K^+ , these are formal local charges, balanced by charge transfer to or from the MnO_2 matrix, in agreement with experimental conditions.

3. Results and Discussion

3.1. Magnetism

Because of the coupling between magnetic ordering, energetics, and structure, it is first necessary to determine a model for the magnetic ordering in α - MnO_2 . We used the GGA+U+J approach discussed above and applied it to several models for the magnetic ordering. For simplicity, we only considered collinear magnetism. The lowest-energy magnetic state found is shown in Fig. 2(b). Not surprisingly, the Mn-Mn coupling between corner-sharing MnO_6 is antiferromagnetic (AFM). The interactions between edge-sharing octahedra in neighboring columns are found to be weakly ferromagnetic. Assuming that the calculated magnetic structure is accurate, thermal fluctuations above cryogenic temperatures would readily randomize the magnetic interactions between edge-sharing columns. While the antiferromagnetic interactions are much stronger, they are constrained in quasi-one-dimensional units formed by the four columns of MnO_6 octahedra that surround a 1x1 tunnel. In analogy with the 1D Ising model, the AFM ordering at room temperature is expected to be only short-range.

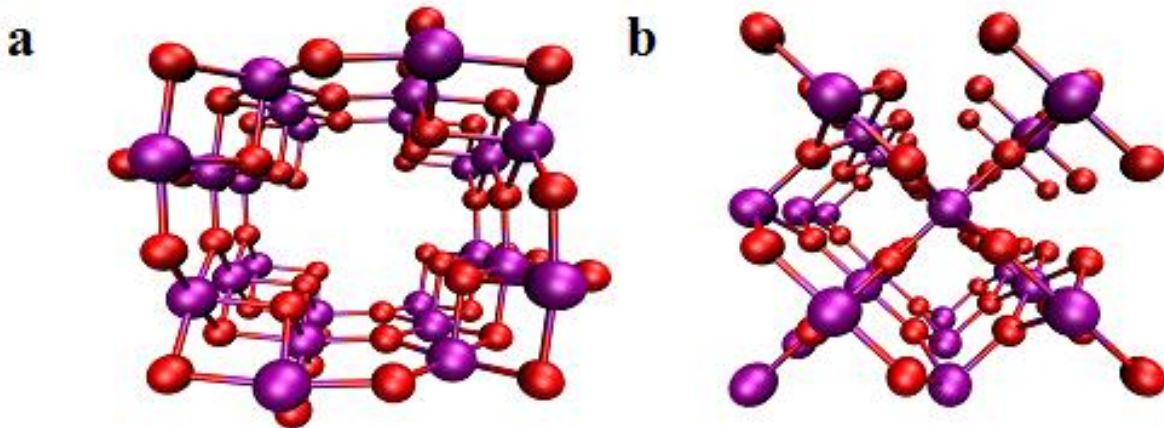


Fig. 3. Crystal structures of (a) α - MnO_2 and (b) β - MnO_2 , Mn in purple and O in red.

3.2. Structure

α - MnO_2 is found to have either a tetragonal structure or a related monoclinic structure with pseudotetragonal symmetry [9]. Gao et al. [11] reported a tetragonal structure at composition $\text{K}_{0.11}\text{MnO}_2[\text{H}_2\text{O},\text{H}_3\text{O}]_{0.07}$ with $a = 9.8241$ and $c = 2.856$ (all unit cell parameters in this work in \AA), whereas a work related to the present study [6] reports a monoclinic cell at composition $\text{K}_{0.09}\text{MnO}_2(\text{H}_2\text{O})_{0.08}$ with $a = 9.8394$, $b = 2.856$, $c = 9.790$, and $\beta = 90.138^\circ$. The different crystal symmetries may be related to the different “dopant” concentrations reported in the two studies. Our minimum-energy calculated structure for pure α - MnO_2 structure is monoclinic with $a = 9.702$, $b = 2.856$, $c = 9.685$, $\beta = 90.041^\circ$ (Fig. 3). The Mn-O bond lengths are all ~ 1.90 \AA . The calculated energy difference between the monoclinic and parent tetragonal structures is only 0.1 meV per

MnO₂ formula unit. Although the calculated structure has a smaller unit cell than the experiment, these calculations are performed without dopants; as shown below, much better agreement is obtained when the dopants are included. In the above-cited monoclinic refinement [6], there are 0.72 K and 0.634 H₂O per unit unit cell of composition Mn₈O₁₆. To mimic the partial occupancy of the dopants with an explicit atomistic model, we use a α -MnO₂ cell tripled along the *b* axis. The experimental stoichiometry is then closely matched by placing 2 K and 2 H₂O within the tripled cell. Before optimizing the arrangement of K and H₂O, we first explore the energetics and electronic structure of α -MnO₂ with K doping alone.

3.3 K dopants

As determined by structure refinements, K⁺ ions in α -MnO₂ fit in the 2x2 tunnels. We find the lowest-energy position of a K⁺ ion to be at the experimental position with eight oxygen near neighbors (Fig. 4 (a)) [6,9,11]. The distances between K⁺ and its closest Mn and O are 3.57 Å and 2.85 Å respectively. The energy of a K⁺ halfway between two neighboring equilibrium positions is 0.37 eV higher. We use this result as an estimate for the energy barrier for K⁺ diffusion in α -MnO₂.

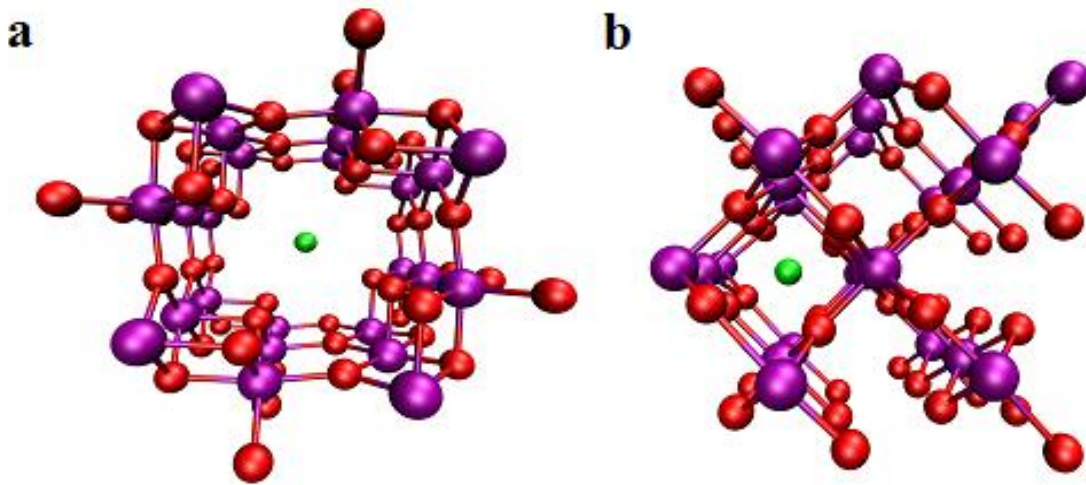


Fig. 4. K-doped α - and β -MnO₂, Mn in purple, O in red and K in green: (a) a cell of K-doped α -Mn₂₄O₄₈ and (b) a cell of K-doped β -Mn₂₄O₄₈.

Formally, the addition of a K⁺ to MnO₂ reduces one Mn⁴⁺ to Mn³⁺. Our calculations show that the electron donated by the K is shared by several Mn leading to noninteger charges on these Mn. We investigated possible electronic structures where the extra electron is initially located on a single Mn, and the environment around this Mn given a Jahn-Teller distortion typical for Mn³⁺ ions [23]. With the ions frozen in this position, the state with a localized electron is found to be electronically stable. Once lattice relaxation is allowed, however, the magnetic structure reverts back to what was found initially. Whether this result is an artifact of the treatment of magnetism in DFT or

whether donated electrons in α -MnO₂ are indeed shared by more than one Mn remains to be resolved.

We next investigated the binding energy of K. Neglecting finite temperature effects, the K-MnO₂ binding energy is computed as

$$E_b = (E_{\text{total, doped}} - E_{\text{total, undoped}} - nE_K) / n \quad (1)$$

where the first two terms refer to the total energies of Mn₂₄O₄₈ with and without K doping, respectively; n specifies the number of K; and E_K is the energy of an individual K atom. The computed binding energy of 4.36 eV implies a strong interaction between K and α -MnO₂.

A related question is the comparative stability of α -MnO₂ and β -MnO₂. We find that β -MnO₂ is more stable by about 20 meV per MnO₂ formula unit, in agreement with the experimental phase diagram. But when K is added, there is no favorable interstitial position in β -MnO₂. The optimal position found is within the 1x1 tunnels (Fig. 4(b)), but that leads to large structural distortions. The distances between K and its closest Mn and O are 2.78 Å and 2.30 Å respectively, much shorter than those in α -MnO₂. For composition K_{1/24}MnO₂, the structure based on the α -phase is 342 meV lower in energy per formula unit than that based on the β -phase. Our results imply a crossover in stability for K _{x} MnO₂ at very low K concentration $x = 0.002$. These results are fully consistent the experimental observations that α -MnO₂ requires dopants for stability.

To further understand the effect of K on α -MnO₂, we study the changes in electronic structure when K is doped into α -MnO₂. Fig. 5 shows the total DOS of undoped α -MnO₂ as well as the DOS of α -MnO₂ after doping with a K atom. The Fermi level (E_f) is shifted to zero in each case. Undoped α -MnO₂ is a semiconductor with the Fermi level inside the band gap. The band gap is 1.33 eV (Fig. 3a). Detailed band structure computations (not shown) show that the highest valence band state is at Γ (the Brillouin zone center) and the lowest conduction band state is a zone-edge state at $\mathbf{k} = (0.5, 0, 0.5)$ in reciprocal lattice units. With K doping, the conduction band of α -MnO₂ is partially filled (Fig. 5(b)). This partial filling of the conduction band is a consequence of electronic charge transfer from K to α -MnO₂. Integrating the DOS of doped α -MnO₂ up to the Fermi energy, the estimated charge transferred toward α -MnO₂ is 1.22 electrons. The band gap decreases slightly to 1.29 eV (for composition K_{1/6}MnO₂). Experimentally, the band gap for cryptomelane is 1.32 eV [11], in excellent agreement with our calculations, demonstrating their predictive power.

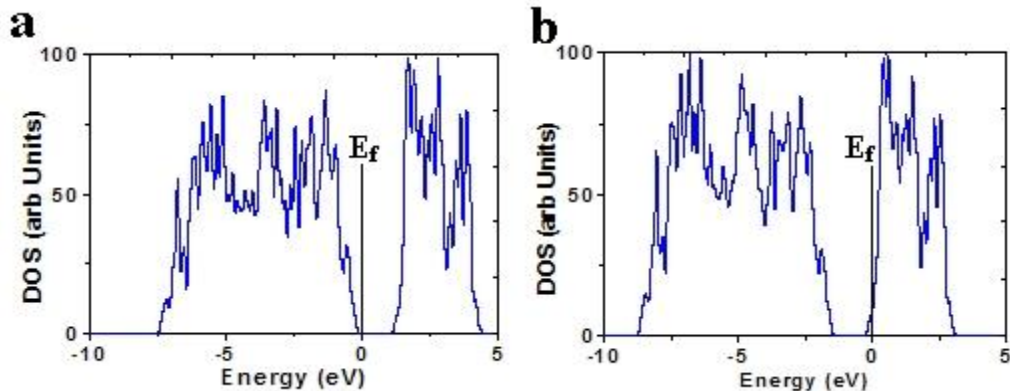


Fig. 5 Electronic structure calculations of undoped and K-doped α -MnO₂, Fermi level $E_f = 0$: (a) Total DOS of undoped α -MnO₂; and (b) DOS of α -MnO₂ after doping with a K atom.

3.4 Interactions of K-doped α -MnO₂ with OH⁻, H₂O and H₃O⁺

According to experimental observations, the synthesis of K-doped α -MnO₂ materials may also incorporate other species such as H₂O in the 2 x 2 tunnels. Since x-ray diffraction can not resolve H positions, there is some question about whether O inside the tunnel occurs as a neutral water molecule or in the form of another hydride such as OH⁻ or H₃O⁺. Gao et al. [11] suggest that H₃O⁺ may be present, possibly because positive cations such as K⁺ tend to occupy the tunnels. On the other hand, many related manganese oxide minerals contain OH⁻ groups [8]. First-principles calculations can help clarify these structural issues.

We started with K₂X₂Mn₂₄O₄₈ structures, where X refers to OH⁻, H₂O or H₃O⁺. We tested all the possible sites for these four adsorbates in the (2 × 2) tunnels using total energy minimization calculations. Placing one K and one OH⁻/H₂O/H₃O⁺ in each of the two empty (2 × 2) tunnels are energetically preferred. Fig. 6 shows the ground-state structure of K₂X₂Mn₂₄O₄₈ (X refers to OH⁻/H₂O/H₃O⁺). Each cell, Mn₂₄O₄₈, contains two K⁺ and OH⁻/H₂O/H₃O⁺ in the (2 × 2) tunnels (Figs. 6(a), (c) & (e)). The axes of the tunnels are the favorable sites for the adsorbates. In the equilibrium state, the O atom of OH⁻/H₂O/H₃O⁺ is positioned closer to the K⁺ ion than the H atom(s) of OH⁻/H₂O/H₃O⁺ (Figs. 6(b), (d) & (f)). Table 1 lists the optimum distance between K and the O atom of OH⁻/H₂O/H₃O⁺. OH⁻ has the closest distance to K⁺, compared to H₂O and H₃O⁺. As seen in Fig. 6(b), OH⁻ bonds with K⁺, and forms a compound of KOH. The K-OH bond length is 2.51 Å. Due to electronic charge repulsion, K⁺ to H₃O⁺ has the longest K-O distance, 3.46 Å. Experimental probes that can measure the K-O distance inside the tunnels should therefore be able to determine whether O is present in the form of H₃O⁺ or not.

The best agreement with the experimental lattice parameters occurs for the model with H₂O in the columns, for which $a = 9.771$, $b/3 = 2.846$, $c = 9.762$, and $\beta = 90.022^\circ$. With van der Waals interactions included, the calculated parameters are $a = 9.779$, $b/3 = 2.843$, $c = 9.741$, $\beta = 90.103^\circ$. It is interesting that including vdW interactions improve the

agreement between the calculated monoclinic distortion and the experiment value, but does not improve the volume. Replacing H₂O with either OH⁻ or H₃O⁺ decreases the predicted cell volume. The decrease in volume for the H₃O⁺ case may be related to a short O-H bond formed by one H in each H₃O⁺ with an O in the MnO₂ framework (Figure 6(e)).

K-doped α -MnO₂-related materials have a potential application in carbon capture and storage [6]. During the synthesis of these materials, H₂O molecules are found in the (2 × 2) tunnels of α -MnO₂. After heating the sample at 150 °C, H₂O can be removed from the sample, but K remains [6]. Our first-principles calculations indicate that the binding energy of H₂O in the α -MnO₂ is 0.39 eV, smaller than that of K by 4 eV. Such a low binding energy implies a weak interaction of H₂O with K-doped α -MnO₂, and that therefore it should be relatively easy to remove H₂O from the α -MnO₂ and related materials. Completely removing H₂O content in the sample increases the adsorption uptake of CO₂ [6].

Adsorbate X	K-O distance (Å)
OH ⁻	2.51
H ₂ O	2.67
H ₃ O ⁺	3.46

Table 1 Optimum distance between K and OH⁻/H₂O/H₃O⁺

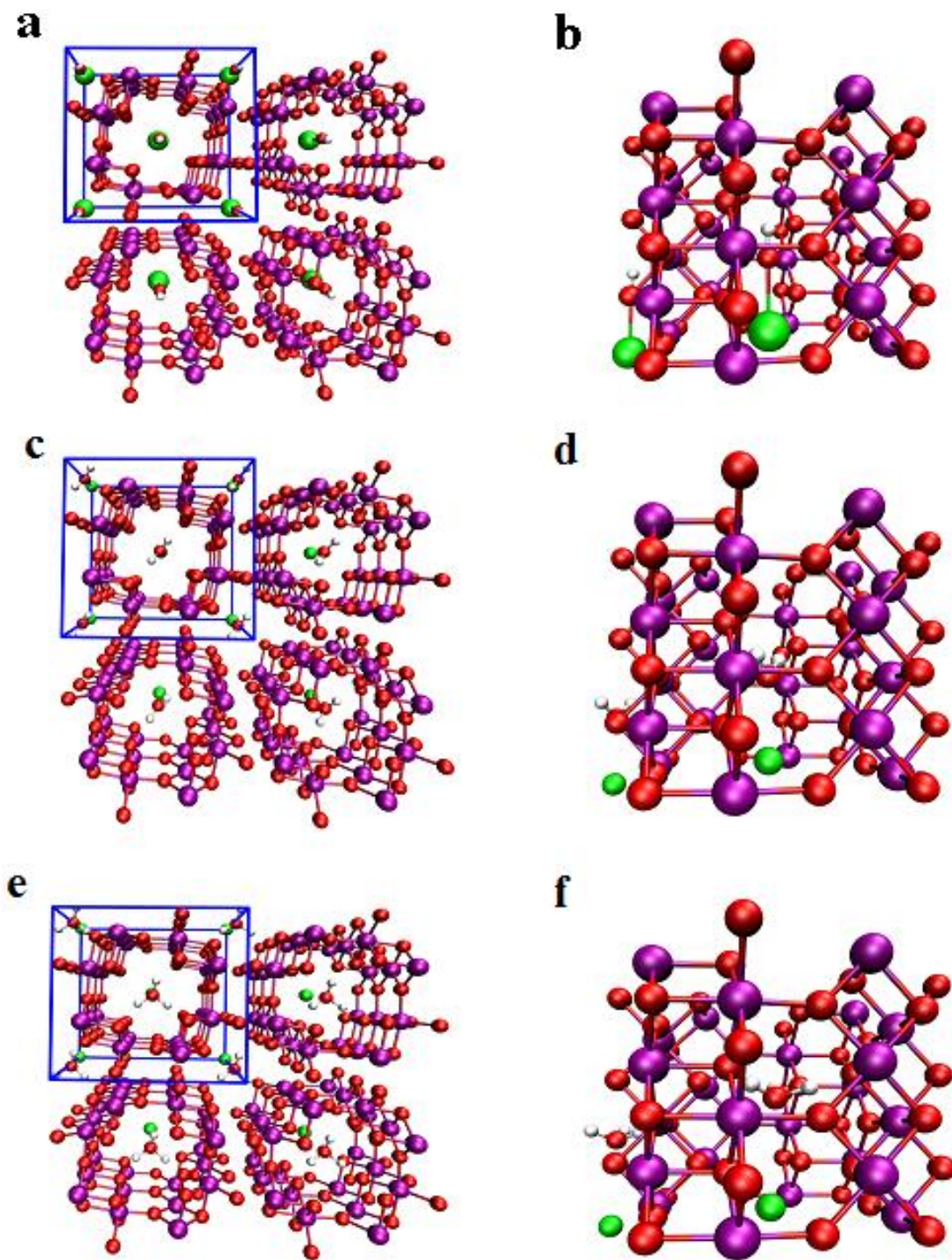


Fig. 6. $K_2X_2Mn_{24}O_{48}$, where X represents $OH^-/H_2O/H_3O^+$, K in green, Mn in purple, O in red and H in white: (a), (c) & (e) (2×2) supercell down tunnel axis; (b) (d) & (f) side view of a single cell.

4. Conclusions

First-principles density functional theory calculations were used to investigate α -MnO₂, a structure containing a framework of corner and edge sharing MnO₆ octahedra with tunnels in between. The calculated 1.3 eV band gap agrees with experiment, demonstrating the predictive power of DFT+U+J for manganese dioxide. The predictions of short-range antiferromagnetism, an indirect bandgap, and optimal K-O distances for tunnels containing both K⁺ and OH⁻, H₂O, or H₃O⁺ show the variety of phenomena that occur in this system, and provide quantitative predictions for comparison with future experiments. Our results provide a benchmark for further computational studies of the technologically important family of manganese oxide materials.

Acknowledgments

We thank W. Wong-Ng and L. Espinal for helpful discussions and W. Wong-Ng for providing us with preliminary crystallographic data on α -MnO₂.

5. References

- [1] M. Toupin, T. Brousse, and D. Belanger, *Chem. Mater.* 14 (2002) 3946.
- [2] X. Wang and Y. Li, *J. Am. Chem. Soc.* 124 (2002) 2880.
- [3] F. Y. Cheng, J. Z. Zhao, W. Song, C. S. Li, H. Ma, J. Chen, and P. W. Shen, *Inorg. Chem.* 45 (2006) 2038.
- [4] S. L. Suib, *Acct. Chem. Res.* 41 (2008) 479.
- [5] S. L. Suib, *J. Mater. Chem.* 18 (2008) 1623.
- [6], L. Espinal, W. Wong-Ng, J. A. Kaduk, A. J. Allen, C. R. Snyder, C. Chiu, D. W. Siderius, L. Li, E. Cockayne, A. E. Espinal, and S. L. Suib, "Time dependent CO₂ sorption hysteresis in a one-dimensional octahedral molecular sieve", unpublished preprint (2011) (and Supplementary Information therein).
- [7] A. N. Grundy and B. Hallstedt, and L. J. Gauckler, *J. Phase Equilib.* 24 (2003) 21.
- [8] C. Klein and C. S. Hulbrut, Jr., *Manual of Mineralogy*, John Wiley & Sons, New York, 1977.
- [9] A. Bystrom and A. M. Bystrom, *Acta Crystollogr.* 3 (1950) 146.

- [10] K.-H. Hellwege and A. M. Hellwege, eds., *Landolt-Bornstein Numerical Data and Functional Relationships in Science and Technology, New Series III.7.b.1*, Springer-Verlag, Berlin, 1975.
- [11] T. Gao, M. Glerup, F. Krumeich, R. Nesper, H. Fjellvag, and P. Norby, *J. Phys. Chem. C* 112 (2008) 13134.
- [12] Y. Li, H.Q. Xie, J.F. Wang, and L.F. Chen, *Materials Letters* 65 (2011) 403.
- [13] H.W. Ma, J.F. Shen, M. Shi, B. Yan, N. Li, and M.X. Ye, *Materials Research Bulletin* 46 (2011) 1461.
- [14] G. Kresse and J. Joubert, *Phys. Rev. B* 59 (1999) 1758.
- [15] P. E. Blochl, *Phys. Rev. B* 50 (2004) 17953.
- [16] J.P. Perdew, A. Ruzsinszky, G.I. Csonka, O.A. Vydrov, G.E. Scuseria, L.A. Constantin, X. Zhou, and K. Burke, *Phys. Rev. Lett.* 100 (2008) 136406.
- [17] C. Franchini, R. Podlucky, J. Paier, M. Marsman, and G. Kresse, *Phys. Rev. B* 75 (2007) 195128.
- [18] Y. Paik, J. P. Osgovic, F. Wang, W. Bowden, and C. P. Grey, *J. Am. Chem. Soc.* 123 (2001) 9367.
- [19] A. I. Liechtenstein, V. I. Anisimov, and J. Zaane, *Phys. Rev. B* 52 (1995) R5467.
- [20] A. K. M. Farid Ul Islam, R. Islam, and K. A. Khan, *J. Mater. Sci.: Mater. Electron.* 16 (2005) 203.
- [21] K. G. Ray and D. Olmsted and N. He and Y. Houndonougbo and B. B. Laird and M. Asta, *Phys. Rev. B* 85 (2012) 085410.
- [22] J. Klimes and D. B. Bowler and A. Michaelides, *Phys. Rev. B* 84 (2011) 195131.
- [23] J. B. Goodenough, *J. Appl. Phys* 81 (1997) 5330.

FIGURE CAPTIONS

Fig. 1 Octahedral molecular sieve MnO_2 structures with alternating 1×1 and $m \times n$ tunnels. (a) $m=1, n=1$ $\beta\text{-MnO}_2$ structure. (b) $m = 2, n=1$. (c) $m=2, n=2$ $\alpha\text{-MnO}_2$ structure. (d) $m=3, n=3$. Mn atoms shown in purple and oxygen octahedral frameworks in red.

Fig. 2 (a) Experimental magnetic structure of $\beta\text{-MnO}_2$. (b) Predicted ground state magnetic structure of $\alpha\text{-MnO}_2$. Octahedra are colored according to the spin state of the central Mn, dark blue for spin “up” and light red for spin “down”. All octahedra in each column have the same spin.

Fig. 3. Crystal structures of (a) $\alpha\text{-MnO}_2$ and (b) $\beta\text{-MnO}_2$, Mn in purple and O in red.

Fig. 4. K-doped α - and $\beta\text{-MnO}_2$, Mn in purple, O in red and K in green: (a) a cell of K-doped $\alpha\text{-Mn}_{24}\text{O}_{48}$ and (b) a cell of K-doped $\beta\text{-Mn}_{24}\text{O}_{48}$.

Fig. 5 Electronic structure calculations of undoped and K-doped $\alpha\text{-MnO}_2$, Fermi level $E_f = 0$: (a) Total DOS of undoped $\alpha\text{-MnO}_2$; and (b) DOS of $\alpha\text{-MnO}_2$ after doping with a K atom.

Fig. 6. $\text{K}_2\text{X}_2\text{Mn}_{24}\text{O}_{48}$, where X represents $\text{OH}^-/\text{H}_2\text{O}/\text{H}_3\text{O}^+$, K in green, Mn in purple, O in red and H in white: (a), (c) & (e) (2×2) supercell down tunnel axis; (b) (d) & (f) side view of a single cell.